COMPUTER METHODS IN APPLIED MECHANICS AND ENGINEERING 26 (1981) 331–362
NORTH-HOLLAND PUBLISHING COMPANY

NONLINEAR FINITE ELEMENT ANALYSIS OF SHELLS: PART I. THREE-DIMENSIONAL SHELLS

Thomas J.R. HUGHES* and Wing Kam LIU**
Division of Engineering and Applied Science, California Institute of Technology, Pasadena, CA 91125, USA

Received 6 May 1980

A nonlinear finite element formulation is presented for the three-dimensional quasistatic analysis of shells which accounts for large strain and rotation effects, and accommodates a fairly general class of nonlinear, finite-deformation constitutive equations. Several features of the developments are noteworthy, namely: the extension of the selective integration procedure to the general nonlinear case which, in particular, facilitates the development of a 'heterosis-type' nonlinear shell element; the presentation of a nonlinear constitutive algorithm which is 'incrementally objective' for large rotation increments, and maintains the zero normal-stress condition in the rotating stress coordinate system; and a simple treatment of finite-rotational nodal degrees-of-freedom which precludes the appearance of zero-energy in-plane rotational modes. Numerical results indicate the good behavior of the elements studied.

1. Introduction

The history of finite element procedures for plate and shell analysis now spans over 20 years. Apparently, it was Papenfuss [40] who developed the first plate bending element. This element is now known to possess a deficiency which renders it nonconvergent. Numerous plate elements have been proposed since Papenfuss' seminal attempt, most of which are convergent and many of which are quite accurate. (The number of efforts along these lines is too great to give individual mention herein. Descriptions and references to many important works may be obtained by consulting standard texts [15, 53], the review article [16], and the thesis [14].) Nevertheless, many successful efforts in the area of plate and shell finite elements have not come simply or easily. In fact, the degree of accuracy achieved generally seems to be attained at the price of considerable complexity. Thus it is fair to say that there is still wide dissatisfaction with available methodology.

When one undertakes the development of a fully general procedure for the nonlinear analysis of shells,[1] the difficulties encountered increase considerably compared with a linear, or limited-generality nonlinear, endeavor. To some extent this is due to the unavailability of a convenient, general enough nonlinear shell theory. It has thus been concluded by many finite element researchers that the development of a fully general nonlinear shell analysis procedure

*Now at Division of Applied Mechanics, Stanford University, Stanford, CA 94305, USA.
**Now at Dept. of Mechanical and Nuclear Engineering, Northwestern University, Evanston, IL 60201, USA.

[1]By a fully general procedure for nonlinear shell analysis, we mean one which accommodates large strains and rotations, and permits use of arbitrary, three-dimensional, nonlinear constitutive equations.

0045–7825/81/0000–0000/$02.50

must circumvent shell theories as a starting point and must begin directly with the fundamental equations of nonlinear continuum mechanics. It is this philosophy which is adopted herein.

Plate bending finite elements provide key conceptual ingredients for the development of shell finite elements. Several years ago, the senior author and colleagues undertook a series of studies of plate bending elements [23–25, 27] based upon Mindlin theory [36]. The studies are revealing in themselves with respect to the linear finite element analysis of plates, but more important from our point of view, they are fundamental to the development of a general nonlinear shell capability. The reason for this is that the hypotheses of Mindlin theory are explicit and unambiguous, and thus may be directly embedded in three-dimensional theory to develop a plate theory. Furthermore, generalizations of the Mindlin hypotheses to the fully-general nonlinear case provides a derivational procedure which enables a shell finite element formulation to be developed circumventing any particular shell theory. This point of view was originally adopted in the linear case by Ahmad et al. [1] and has been subsequently used by many investigators. Recent works in the nonlinear area which may be mentioned are [8, 14, 29, 41, 42, 45]. This technique has been termed the "degenerated shell element procedure" since three-dimensional theory is reduced, or degenerated, to a shell theory simultaneously with the finite element discretization.

Certain fundamental difficulties nevertheless remain, and this paper addresses itself in part to some of these problems. In this regard, we view the present work as taking several steps toward the development of optimal, fully-general nonlinear quasistatic shell analysis. In particular, certain problems associated with finite element procedures in this area are resolved herein. These are described as follows:

The salubrious effects of reduced integration techniques on isoparametric plate and shell elements have been established in a number of investigations (see, e.g., [23–25, 27, 29, 30, 34, 35, 38, 41, 42, 44, 47, 53–55]). For the lower-order elements, reduced integration appears to be absolutely essential for good behavior in thin-plate applications; for the higher-order elements, significant improvements in accuracy are attained by reduced integration. Uniform application of reduced integration, on the other hand, tends to diminish the rank of elemental matrices and may occasionally lead to spurious zero-energy modes appearing in the global equations. An alternative prodecure, known as selective integration, maintains the attributes of reduced integration while mitigating rank-deficiency problems. In this procedure, reduced integration is employed on the troublesome, transverse-shear terms, and 'normal' integration is retained for the bending terms. Selective integration procedures for plates and shells have been studied in [13, 20, 23–25, 27, 29, 30, 34, 35, 38, 41, 42, 44]. The use of selective integration in association with specific interpolatory patterns has led to correct-rank, high-accuracy plate elements [20, 23, 24], termed 'heterosis elements'.

A shortcoming of the classical selective integration procedure has been noted in that implementation requires an explicit segregation of transverse-shear terms from other effects. When the material model is linear and isotropic, for example, an explicit segregation may be performed and thus no difficulties are encountered. However, in more general anisotropic and nonlinear situations the segregation of effects is no longer possible in that full coupling may exist. The situation is analogous to that for anisotropic and nonlinear, nearly-incompressible continuum applications. A generalization of the classical selective integration procedure which accommodates this case has been recently proposed [20, 21]. Herein we describe a similar extension which enables the attributes of selective integration to be attained in anisotropic and

nonlinear plate and shell problems. In particular, this development facilitates the formulation of a general, nonlinear shell element of the heterosis type.

In a general nonlinear shell formulation, it is most convenient if constitutive equations are written with respect to coordinate axes naturally defined by the shell geometry. Herein we adopt a so-called 'lamina' coordinate system at each stress storage point for this purpose. The lamina systems are different, in general, from point-to-point within an element, and undergo finite rotations in the course of the solution process. Thus it is imperative that special consideration be given to the integration of constitutive equations to achieve physically meaningful, accurate response.

We present a numerical algorithm for integrating constitutive equations, in the presence of arbitrarily large deformations, which possesses two important features: First, the algorithm is 'incrementally objective', that is, for large rigid rotations of stress-point neighborhoods, exact stress updates are attained. This ensures that when large rotations are experienced, no spurious stressing will develop, and is in keeping with the 'objectivity' of well-set finite-deformation constitutive equations [49]. A related development for the nonlinear continuum case, in which the referential coordinate axes are fixed, has been presented in [28].

The second feature of the integration is that the normal-stress component (with respect to the rotating lamina through the stress-point) is continuously constrained to be zero for three-dimensional constitutive equations. This overcomes the artificial stiffening induced by the hypothesis that 'fibers' are inextensible, and is in keeping with classical plate/shell theory assumptions which are typically invoked in simpler settings. This allows the shell elements to use general, three-dimensional, nonlinear constitutive routines without first modifying the constitutive equations to manifest the zero normal-stress condition, a difficult, it not impossible task in many nonlinear cases.

A by-product of the constitutive algorithm presented is that it sheds light on the 'corotational approximation' [10–12] and clearly delineates when this economical option may be invoked for general element types.

It is a well-known fact that finite rotation components are not vectorial. In geometrically nonlinear analysis this has led to the adoption of several different types of nodal rotational degrees of freedom [4, 12, 19, 29, 52]. In the present formulation we have endeavored to adopt rotational degrees-of-freedom that are natural generalizations of those used in the linear case, namely, the vectorial rotation increments. We begin by specifying the rotation of a node by the position of a unit vector attached to the node pointing in the fiber direction. The incremental components of the displacement of this vector may be identified with classical rotation increments. Furthermore, a coordinate system may be constructed at each node such that the rotation increment about the fiber direction may be eliminated. This procedure facilitates the construction of a five degree-of-freedom nodal system, and consequently precludes rank-deficiency problems associated with the in-plane rotational mode, which have complicated some previous formulations (see, e.g., [30]).

If beam stiffeners are to be employed, the six degree-of-freedom nodal system may be retained in which case the in-plane rotational modes are stabilized by the stiffeners. The decision as to which nodal system is to be used may be made on a node-by-node basis. Thus the attributes of each are available in the present formulation.

An outline of the remainder of the paper is given as follows: In section 2 we describe the geometric and kinematic behavior of a typical shell element. The construction of lamina and

fiber coordinate systems is derived along with the transformation arrays which relate these systems to the global frame. The integration of constitutive equations in the rotating lamina frames is presented in section 3. The definitions of element arrays are presented in section 4. In this section, among other things, we describe the generalization of the selective integration procedure to the anisotropic and nonlinear case; we show how the zero normal-stress condition may be embedded in the definition of the tangent stiffness; and we present a procedure for incorporating shear correction factors. In section 5 we describe the formulation of the global matrix equations and in section 6 we discuss the reduced integration Lagrange elements and heterosis element. Sample problems involving a number of the elements are contained in section 7, and conclusions and recommendations for further research are presented in section 8. Some possible additional refinements in the selective integration procedure are discussed in Appendix A.

2. Geometric and kinematic descriptions

Background information on differential geometry may be found in [39]. A good reference for classical rotation theory is [43]. The basic ideas concerning the development of geometric and kinematic descriptions for shells may be found in [37].

2.1. Geometry

The initial geometry of a typical quadrilateral shell element is defined by the following relations:

$$\boldsymbol{x}(\xi, \eta, \zeta) = \bar{\boldsymbol{x}}(\xi, \eta) + \boldsymbol{X}(\xi, \eta, \zeta), \tag{2.1}$$

$$\bar{\boldsymbol{x}}(\xi, \eta) = \sum_{a=1}^{n_{en}} N_a(\xi, \eta)\bar{\boldsymbol{x}}_a, \tag{2.2}$$

$$\boldsymbol{X}(\xi, \eta, \zeta) = \sum_{a=1}^{n_{en}} N_a(\xi, \eta)\boldsymbol{X}_a(\zeta), \tag{2.3}$$

$$\boldsymbol{X}_a(\zeta) = z_a(\zeta)\hat{\boldsymbol{X}}_a \quad \text{(no sum)}, \tag{2.4}$$

$$z_a(\zeta) = N_+(\zeta)z_a^+ + N_-(\zeta)z_a^-, \tag{2.5}$$

$$N_+(\zeta) = \tfrac{1}{2}(1+\zeta), \qquad N_-(\zeta) = \tfrac{1}{2}(1-\zeta). \tag{2.6}$$

In (2.1)–(2.6), $\boldsymbol{x}$ denotes the position vector of a generic point of the shell; $\bar{\boldsymbol{x}}$ is the position vector of a point in the reference surface; $\boldsymbol{X}$ is a position vector based at a point in the reference surface which defines the 'fiber direction' through the point; $\bar{\boldsymbol{x}}_a$ is the position vector of nodal point a; N_a denotes a two-dimensional shape function associated with node a; n_{en} is the number of element nodes; $\hat{\boldsymbol{X}}_a$ is a unit vector emanating from node a in the fiber direction; and z_a is a 'thickness function', associated with node a, which is defined by the location of the reference surface.

Equations (2.1)–(2.6) represent a smooth mapping of the biunit cube into the physical shell domain; see fig. 1. For ζ fixed, the surface defined by (2.1) is called a *lamina*; for ξ, η fixed,

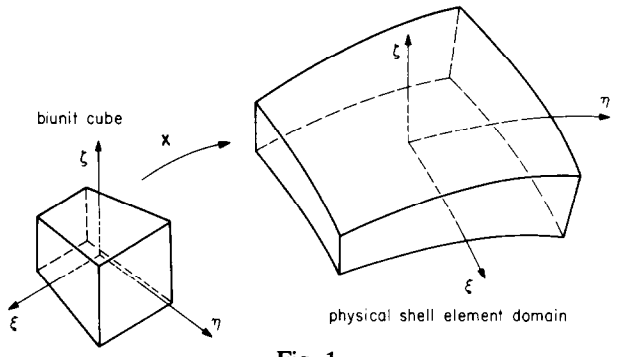

Fig. 1.

the line defined by (2.1) is called a *fiber*. The fibers are not generally perpendicular to the laminae.

For a particular choice of two-dimensional shape functions, (2.1)–(2.6) are precisely defined upon specification of $\bar{\boldsymbol{x}}_a$, $\hat{\boldsymbol{X}}_a$, z_a^+, and z_a^- ($a = 1, 2, \ldots, n_{en}$). We have found it convenient in practice to take as input the coordinates of the top and bottom surfaces of the shell along each nodal fiber ($\boldsymbol{x}_a^+$ and $\boldsymbol{x}_a^-$, resp.) and a parameter $\bar{\zeta} \in [-1, +1]$ which defines the location of the reference surface. For example, if $\bar{\zeta} = -1, 0, +1$ (resp.), then the reference surface is taken to be the bottom, middle, top (resp.) of the shell. This option enables compatible modeling of shell-continuum interfaces. From these data we may calculate

$$\bar{\boldsymbol{x}}_a = \tfrac{1}{2}(1 - \bar{\zeta})\boldsymbol{x}_a^- + \tfrac{1}{2}(1 + \bar{\zeta})\boldsymbol{x}_a^+, \tag{2.7}$$

$$\hat{\boldsymbol{X}}_a = (\boldsymbol{x}_a^+ - \boldsymbol{x}_a^-)/\|\boldsymbol{x}_a^+ - \boldsymbol{x}_a^-\|, \tag{2.8}$$

$$z_a^+ = \tfrac{1}{2}(1 - \bar{\zeta})\|\boldsymbol{x}_a^+ - \boldsymbol{x}_a^-\|, \tag{2.9}$$

$$z_a^- = -\tfrac{1}{2}(1 + \bar{\zeta})\|\boldsymbol{x}_a^+ - \boldsymbol{x}_a^-\|, \tag{2.10}$$

where $\|\cdot\|$ denotes the Euclidean norm (i.e., $\|\boldsymbol{x}\| = (x_1^2 + x_2^2 + x_3^2)^{1/2}$). An illustration of these ideas is presented in fig. 2.

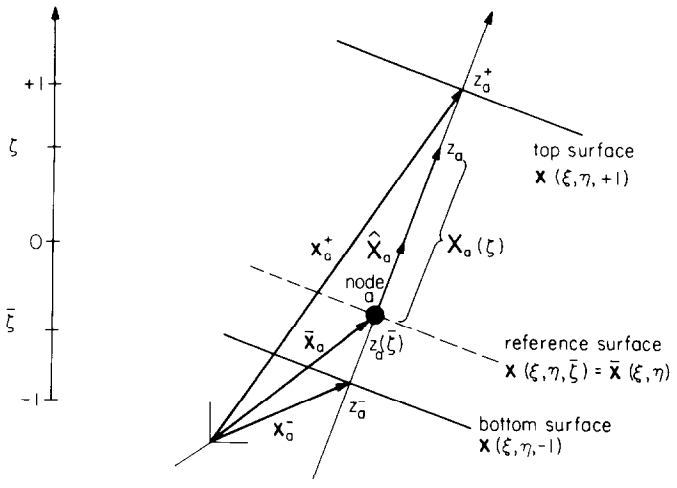

Fig. 2.

The top- and bottom-surface coordinates are uniquely defined at element interfaces. Consequently, there are no gaps or overlaps along element boundaries.

2.2. Kinematics

The kinematics of the shell element are defined by invoking the isoparametric hypothesis that the same expressions are used for kinematics as for geometry with displacement variables in place of coordinate variables. This assumption leads to (cf. (2.1)–(2.4), resp.):

$$\boldsymbol{u}(\xi, \eta, \zeta) = \bar{\boldsymbol{u}}(\xi, \eta) + \boldsymbol{U}(\xi, \eta, \zeta), \tag{2.11}$$

$$\bar{\boldsymbol{u}}(\xi, \eta) = \sum_{a=1}^{n_{en}} N_a(\xi, \eta)\bar{\boldsymbol{u}}_a, \tag{2.12}$$

$$\boldsymbol{U}(\xi, \eta, \zeta) = \sum_{a=1}^{n_{en}} N_a(\xi, \eta)\boldsymbol{U}_a(\zeta), \tag{2.13}$$

$$\boldsymbol{U}_a(\zeta) = z_a(\zeta)\hat{\boldsymbol{U}}_a \quad \text{(no sum)}, \tag{2.14}$$

where $\boldsymbol{u}$ is the displacement of a generic point; $\bar{\boldsymbol{u}}$ is the displacement of a point on the reference surface; and $\boldsymbol{U}$ is the 'fiber displacement'. A general representation of the motion is shown in fig. 3.

The following notations will be employed to represent the deformed geometry:

$$\boldsymbol{y} = \bar{\boldsymbol{y}} + \boldsymbol{Y}, \tag{2.15}$$

$$\bar{\boldsymbol{y}} = \bar{\boldsymbol{x}} + \bar{\boldsymbol{u}}, \tag{2.16}$$

$$\bar{\boldsymbol{y}}_a = \bar{\boldsymbol{x}}_a + \bar{\boldsymbol{u}}_a, \tag{2.17}$$

$$\boldsymbol{Y} = \boldsymbol{X} + \boldsymbol{U}, \tag{2.18}$$

$$\boldsymbol{Y}_a = \boldsymbol{X}_a + \boldsymbol{U}_a, \tag{2.19}$$

$$\hat{\boldsymbol{Y}}_a = \hat{\boldsymbol{X}}_a + \hat{\boldsymbol{U}}_a. \tag{2.20}$$

The nodal fibers are assumed to be inextensible, i.e., they may rotate, but cannot stretch or

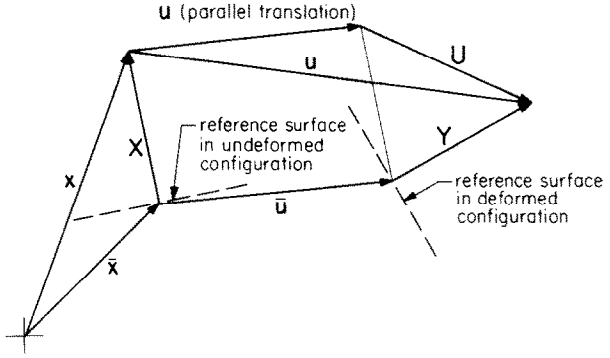

Fig. 3.

contract. Analytically, this condition is maintained by requiring

$$\|\hat{\boldsymbol{Y}}_a\| = 1. \tag{2.21}$$

In practice, a trial value of $\hat{\boldsymbol{U}}_a$ is calculated (i.e., $\hat{\boldsymbol{U}}_a^{\text{trial}}$) and projected radially to maintain (2.21). The steps in the procedure are as follows (see fig. 4):

$$\hat{\boldsymbol{Y}}_a = (\hat{\boldsymbol{X}}_a + \hat{\boldsymbol{U}}_a^{\text{trial}})/\|\hat{\boldsymbol{X}}_a + \hat{\boldsymbol{U}}_a^{\text{trial}}\|, \tag{2.22}$$

$$\hat{\boldsymbol{U}}_a = \hat{\boldsymbol{Y}}_a - \hat{\boldsymbol{X}}_a. \tag{2.23}$$

The use of trigonometric representations for rotational degrees-of-freedom (see, e.g., [41, 45]) is thus obviated. We have found the present scheme to be both economical and effective in practice.

2.3. Lamina coordinate systems

At each integration point in the element, a Cartesian reference frame is erected so that two axes are tangent to the lamina through the point. The frame is defined by its orthonormal basis vectors $\boldsymbol{e}_1^l$, $\boldsymbol{e}_2^l$, $\boldsymbol{e}_3^l$ which are calculated as follows (see fig. 5):

$$\boldsymbol{e}_1^l = \boldsymbol{y}_{,\xi}/\|\boldsymbol{y}_{,\xi}\|, \tag{2.24}$$

$$\boldsymbol{e}_3^l = \boldsymbol{e}_1^l \times \boldsymbol{y}_{,\eta}/\|\boldsymbol{e}_1^l \times \boldsymbol{y}_{,\eta}\|, \tag{2.25}$$

$$\boldsymbol{e}_2^l = \boldsymbol{e}_3^l \times \boldsymbol{e}_1^l, \tag{2.26}$$

where a comma is used to denote partial differentiation (e.g., $\boldsymbol{y}_{,\xi} = \partial \boldsymbol{y}/\partial \xi$) and '$\times$' denotes the cross product. Note that $\boldsymbol{e}_1^l$ and $\boldsymbol{e}_2^l$ are tangent to the lamina, and $\boldsymbol{e}_1^l$ is tangent to η = const. lines; $\boldsymbol{e}_2^l$ is generally not tangent to ξ = const. lines. The lamina basis rotates rigidly as the element deforms.

It may be observed that $\boldsymbol{e}_3^l$ is not generally tangent to the fiber direction at the integration point; see fig. 6. We use the $\boldsymbol{e}_3^l$ direction for purposes of invoking the plane stress hypothesis.

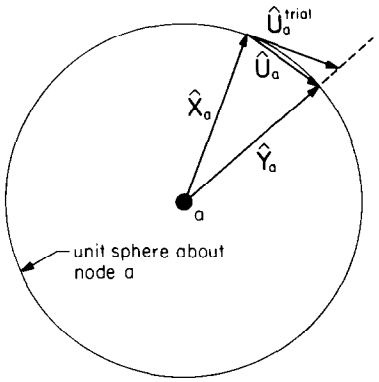

Fig. 4. Nodal fiber inextensibility condition maintained by radial return normalization.

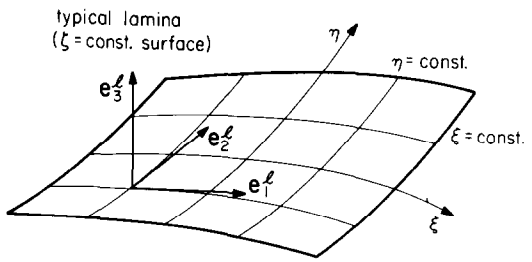

Fig. 5. Typical lamina coordinate system.

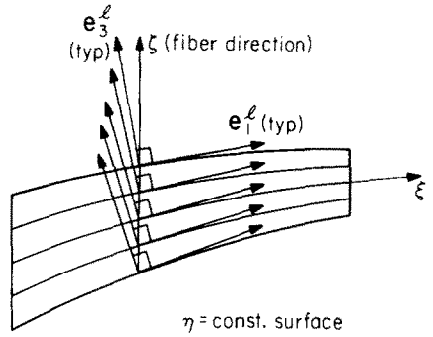

Fig. 6. Lamina coordinate systems along a fiber.

In the sequel, it will be necessary to transform quantities from the global coordinate system to the lamina system. This is facilitated by the following matrix:

$$\boldsymbol{q} = [\boldsymbol{e}_1^l \boldsymbol{e}_2^l \boldsymbol{e}_3^l]^t\text{: global} \rightarrow \text{lamina}, \tag{2.27}$$

in which the superscript 't' denotes transpose. Clearly, $\boldsymbol{q}$ is orthogonal.

2.4. Fiber coordinate systems

At each node a unique local Cartesian coordinate system is constructed which is used as a reference frame for rotation increments. The only requirement that the frame must satisfy is that one direction coincide with the fiber direction. This in itself is not sufficient to define the frame. For this purpose the following algorithm is employed:

Let $\hat{\boldsymbol{Y}}$ denote the unit basis vector in the fiber direction. (We omit the nodal subscript 'a' throughout this discussion for notational clarity.) Let $\boldsymbol{e}_1$, $\boldsymbol{e}_2$, $\boldsymbol{e}_3$ denote the global Cartesian basis, i.e.,

$$\boldsymbol{e}_1 = \begin{bmatrix} 1 \\ 0 \\ 0 \end{bmatrix}, \qquad \boldsymbol{e}_2 = \begin{bmatrix} 0 \\ 1 \\ 0 \end{bmatrix}, \qquad \boldsymbol{e}_3 = \begin{bmatrix} 0 \\ 0 \\ 1 \end{bmatrix}. \tag{2.28}$$

The global Cartesian components of $\hat{\boldsymbol{Y}}$ are denoted $\hat{Y}_i$, $i = 1, 2, 3$.

Algorithm

Step 1. Let $a_i = |\hat{Y}_i|$, $i = 1, 2, 3$. (2.29)

Step 2. $j = 1$. (2.30)

Step 3. If $a_1 > a_3$, then $a_3 = a_1$, and $j = 2$. (2.31)

Step 4. If $a_2 > a_3$, $j = 3$. (2.32)

Step 5. $\boldsymbol{e}_3^f = \hat{\boldsymbol{Y}}$. (2.33)

Step 6. $\boldsymbol{e}_2^f = (\hat{\boldsymbol{Y}} \times \boldsymbol{e}_j)/\|\hat{\boldsymbol{Y}} \times \boldsymbol{e}_j\|$. (2.34)

Step 7. $\boldsymbol{e}_1^f = \boldsymbol{e}_2^f \times \hat{\boldsymbol{Y}}$. (2.35)

The orthonormal fiber basis obtained (i.e., $\boldsymbol{e}_1^f$, $\boldsymbol{e}_2^f$, $\boldsymbol{e}_3^f$) satisfies the condition that if $\hat{\boldsymbol{Y}}$ is 'close' to $\boldsymbol{e}_3$, then $\boldsymbol{e}_1^f$, $\boldsymbol{e}_2^f$, $\boldsymbol{e}_3^f$ will be 'close' to $\boldsymbol{e}_1$, $\boldsymbol{e}_2$, $\boldsymbol{e}_3$, respectively (see fig. 7). The fiber basis rotates rigidly with the nodal fiber.

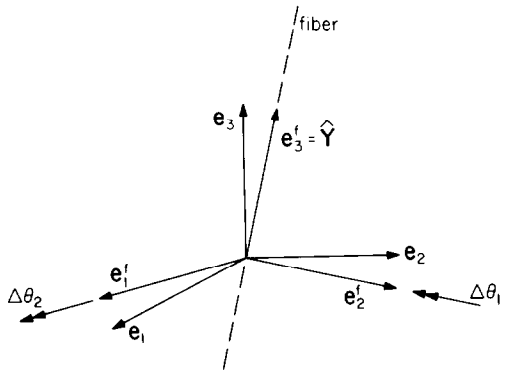

Fig. 7. Nodal fiber basis.

It is necessary in what follows to transform quantities from the nodal fiber system to the lamina system. This may be done with the orthogonal matrix $\boldsymbol{r}$ defined as follows:

$$\boldsymbol{r}: \quad \text{fiber} \rightarrow \text{lamina}, \tag{2.36}$$

$$\boldsymbol{r} = [r_{ij}]; \quad r_{ij} = \boldsymbol{e}_i^l \cdot \boldsymbol{e}_j^f. \tag{2.37}$$

In (2.37), the dot '·' denotes inner product. If it is important to keep track of the particular node to which $\boldsymbol{r}$ is associated (e.g., 'a'), then a subscript will be added (e.g., $\boldsymbol{r}_a$).

Let $\Delta\theta_1$ and $\Delta\theta_2$ denote rotation increments about the basis vectors $\boldsymbol{e}_2^f$ and $\boldsymbol{e}_1^f$, respectively. The sign convention is defined in fig. 7. The linearized relationship between the components of $\Delta\hat{\boldsymbol{U}}$ in the fiber system (namely, $\Delta\hat{U}_1^f$, $\Delta\hat{U}_2^f$, $\Delta\hat{U}_3^f$) and the incremental rotations, takes on a particularly simple form:

$$\begin{bmatrix} \Delta\hat{U}_1^f \\ \Delta\hat{U}_2^f \\ \Delta\hat{U}_3^f \end{bmatrix} = \begin{bmatrix} -1 & 0 \\ 0 & -1 \\ 0 & 0 \end{bmatrix} \begin{bmatrix} \Delta\theta_1 \\ \Delta\theta_2 \end{bmatrix}. \tag{2.38}$$

Equation (2.38) enables the reduction of the nodal degrees-of-freedom from six to five in the matrix incremental equilibrium equations. This obviates the need to develop artificial in-plane torsional stiffnesses to numerically stabilize rotations about the fiber direction (see [30] for a detailed study of techniques of this kind).

We may also conclude from (2.38) that the components of $\Delta\hat{\boldsymbol{U}}$ in an arbitrary coordinate system may be identified with the incremental rotations in that system.

When beam-type stiffeners are assembled with shell elements, the bending stiffness of the beam naturally provides the in-plane torsional stiffness of the composite structure. In this case six degrees-of-freedom are retained in the global incremental equilibrium equations. It is generally most convenient in this situation to leave the $\Delta\hat{\boldsymbol{U}}$ degrees-of-freedom in the global reference frame.

It also becomes necessary in the formulation of element arrays to transform between the global and nodal fiber coordinate systems. For this purpose we introduce the orthogonal transformation matrix $\boldsymbol{s}$ defined by

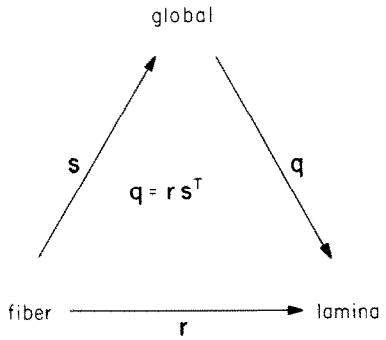

Fig. 8. Commutative diagram depicting the relationship between transformation matrices.

$$\boldsymbol{s} = [\boldsymbol{e}_1^f \boldsymbol{e}_2^f \boldsymbol{e}_3^f]: \quad \text{fiber} \rightarrow \text{global}. \tag{2.39}$$

If necessary, a nodal subscript is introduced (e.g., 'a') to emphasize the particular nodal fiber coordinate system to which $\boldsymbol{s}$ is associated (e.g., $\boldsymbol{s}_a$).

The relationship between the three orthogonal transformation matrices, $\boldsymbol{q}$, $\boldsymbol{r}$, and $\boldsymbol{s}$, may be summarized by a commutative diagram as shown in fig. 8. Thus it may be concluded that

$$\boldsymbol{q} = \boldsymbol{r}\boldsymbol{s}^{\mathrm{t}}. \tag{2.40}$$

3. Constitutive equations

It is convenient to employ rate constitutive equations in the implementation. Equations of this type are used in many theories of engineering interest. As examples, we may mention plasticity, viscoelasticity, and viscoplasticity. In addition, nonlinear elasticity can be put into this form by time-differentiating the more usual forms. Rate constitutive equations facilitate maintaining the zero normal-stress condition incrementally. However, in the present circumstances, the integration of rate constitutive equations requires special considerations in two respects: First, the stress components are referred to a rotating basis—the lamina basis. Second, the zero normal-stress constraint needs to be enforced with respect to the 3-direction of the lamina basis.

3.1. A class of rate constitutive equations

We consider a class of inviscid rate-type constitutive equations which is sufficiently general for the developments herein. With respect to a *fixed* coordinate system, the constitutive equations under consideration take the following form:

$$\dot{\sigma}_{ij} = \bar{c}_{ijkl} v_{(k,l)} + s_{ijkl} v_{[k,l]}, \tag{3.1}$$

in which

$$v_{(k,l)} = (v_{k,l} + v_{l,k})/2, \tag{3.2}$$

$$v_{[k,l]} = (v_{k,l} - v_{l,k})/2, \tag{3.3}$$

$$s_{ijkl} = (\sigma_{il}\delta_{jk} + \sigma_{jl}\delta_{ik} - \sigma_{ik}\delta_{jl} - \sigma_{jk}\delta_{il})/2, \tag{3.4}$$

where σ_{ij} is the Cauchy stress tensor; v_i is the velocity vector; δ_{ij} is the Kronecker delta; a comma is used to denote partial differentiation (e.g., $v_{k,l} = \partial v_k/\partial y_l$); a superposed dot denotes the material time derivative in which material particles are held fixed; and the summation convention is assumed to be in effect for repeated indices i, j, k, and l. The first term on the right-hand side of (3.1) represents the material response due to deformation, whereas the second term accounts for rotational effects. The tensor $\bar{c}_{ijkl}$ is a material response tensor which typically depends upon the stresses, deformation gradient, and material parameters. The tensor s_{ijkl} is uniquely specified by 'objectivity' which requires that the stress-rate (i.e., $\dot{\sigma}_{ij}$) transforms properly under time-dependent rigid rotations. Rate equations of the form (3.1) are frequently used in large-deformation, finite element and finite difference computer programs. A more detailed discussion of equations of this type may be found in [22].

3.2. Numerical algorithm

In a typical time step, the configuration of the body at step $n+1$ may be written as a function of the configuration at step n and the step length Δt, viz.

$$\boldsymbol{y}^{n+1} = \boldsymbol{y}^{n+1}(\boldsymbol{y}^n, \Delta t). \tag{3.5}$$

The displacement increment over the step is

$$\boldsymbol{\delta} = \boldsymbol{y}^{n+1} - \boldsymbol{y}^n. \tag{3.6}$$

Consider the following 'midpoint' configuration

$$\boldsymbol{y}^{n+1/2} = (\boldsymbol{y}^n + \boldsymbol{y}^{n+1})/2. \tag{3.7}$$

Let $\boldsymbol{G}$ denote the gradient of $\boldsymbol{\delta}$ with respect to $\boldsymbol{y}^{n+1/2}$. In component form

$$G_{ij} = \partial \delta_i/\partial y_j^{n+1/2}. \tag{3.8}$$

Strain and rotation increments may be defined in terms of $\boldsymbol{G}$ as follows:

$$\boldsymbol{\gamma} = (\boldsymbol{G} + \boldsymbol{G}^t)/2, \tag{3.9}$$

$$\boldsymbol{\omega} = (\boldsymbol{G} - \boldsymbol{G}^t)/2, \tag{3.10}$$

in which a superscript t denotes transpose. $\boldsymbol{\gamma}$ and $\boldsymbol{\omega}$ represent discrete approximations to the time integrals over the step of the symmetric and skew-symmetric parts of the velocity gradients, respectively.

The orientations of the lamina bases at times t_n and t_{n+1} are defined by (resp.):

$$\boldsymbol{q}^n: \quad \text{global} \to \text{lamina at } t_n, \tag{3.11}$$

$$\boldsymbol{q}^{n+1}: \quad \text{global} \to \text{lamina at } t_{n+1}. \tag{3.12}$$

Consequently, the incremental transformation between lamina bases is given by

$$\Delta \boldsymbol{q} = \boldsymbol{q}^{n+1}(\boldsymbol{q}^n)^{\mathrm{t}}: \quad \text{lamina at } t_n \to \text{lamina at } t_{n+1}. \tag{3.13}$$

(The calculation of $\Delta \boldsymbol{q}$ does not require separate 'shape function' evaluations, since only derivatives with respect to ξ and η are involved; see (2.24)–(2.27).)

In developing a discrete algorithm based upon (3.1), we assume that (3.1) is written with respect to the lamina coordinate system at time t_{n+1}. Furthermore, we assume that the stress components at time t_n are defined with respect to the t_n-lamina system and that $\sigma_{33}^n = 0$.

Consider the following algorithm for integrating (3.1):

$$\bar{\boldsymbol{\sigma}}^{n+1} = \boldsymbol{R}\boldsymbol{\sigma}^n\boldsymbol{R}^{\mathrm{t}}, \tag{3.14}$$

$$\boldsymbol{\sigma}^{n+1} = \bar{\boldsymbol{\sigma}}^{n+1} + \Delta\boldsymbol{\sigma}, \tag{3.15}$$

where

$$\boldsymbol{R} = (\boldsymbol{I} + (\boldsymbol{I} - \tfrac{1}{2}\boldsymbol{\omega})^{-1}\boldsymbol{\omega})\Delta\boldsymbol{q}, \tag{3.16}$$

$$\Delta\sigma_{ij} = \bar{c}_{ijkl}\gamma_{kl}, \tag{3.17}$$

in which $\boldsymbol{I}$ is the identity matrix and

$$\gamma_{33} = -\left(\bar{\sigma}_{33}^{n+1} + \sum_{ij \neq 33} \bar{c}_{33ij}\gamma_{ij}\right) \Big/ \bar{c}_{3333}. \tag{3.18}$$

N.B. All quantities in (3.14)–(3.18), with the exception of $\boldsymbol{\sigma}^n$, are referred to the t_{n+1}-lamina basis.

The matrix $\boldsymbol{R}$ is in general an approximation to the rotation of the material particle relative to the lamina basis. The originally calculated value of γ_{33} is replaced by the value obtained in (3.18) to insure satisfaction of the zero normal-stress condition in the lamina basis at t_{n+1} (i.e., $\sigma_{33}^{n+1} = 0$).

From results obtained in [28] it follows that if the material particle in question is subjected to a rigid motion, that is, if locally

$$\boldsymbol{y}^{n+1} = \Delta\boldsymbol{q}^{\mathrm{t}}\boldsymbol{y}^n, \tag{3.19}$$

then

$$\boldsymbol{R} = \boldsymbol{I} \tag{3.20}$$

and

$$\boldsymbol{\gamma} = \boldsymbol{0}, \tag{3.21}$$

where **0** is the zero matrix. (This result holds for particle rotations not equal to 180°; see [28] for further details.) Consequently, for large rigid-rotation increments, exact results are obtained by (3.14)–(3.18), i.e.,

$$\boldsymbol{\sigma}^{n+1} = \boldsymbol{\sigma}^{n}. \tag{3.22}$$

We refer to an algorithm which exhibits this feature as being 'incrementally objective'.

REMARK 1. Subincremental algorithms are often advocated for use in integrating rate constitutive equations (see, e.g., [46]). The preceding algorithm may be generalized to a subincremental one by repeating the calculations involved in (3.5)–(3.18) within each subincrement.

REMARK 2. In plasticity, the $\bar{c}_{ijkl}$'s are functions of the stresses. It is appropriate in this situation to use the rotated stresses (i.e., $\bar{\boldsymbol{\sigma}}^{n+1}$) to evaluate the $\bar{c}_{ijkl}$'s. On the other hand, if a 'radial return' implementation [32, 33] is employed, then the $\bar{c}_{ijkl}$'s would be simply the elastic coefficients and $\boldsymbol{\sigma}^{n+1}$ would play the role of an elastic trial stress. In this case, if $\boldsymbol{\sigma}^{n+1}$ was exterior to the yield surface, then it would be projected radially onto the yield surface in the plane $\sigma_{33} = 0$.

REMARK 3. In many situations of practical interest, the particle rotation will be very close to the rotation of the lamina basis and thus $\boldsymbol{R} \simeq \boldsymbol{I}$. This is the case for what is classically known as the 'small strain-finite rotation' approximation. In this case the lamina coordinate system rotates with the particle (i.e., is 'corotational') and thus the calculations involving $\boldsymbol{R}$ may be omitted. This philosophy has been exploited in the works of Argyris [2–4, 6], Belytschko [10–12] and Wempner [51].

4. Element arrays

4.1. Material tangent matrix

In general *three-dimensional analysis*, we adopt use of the following material tangent matrix:

$$\boldsymbol{D} = \begin{bmatrix} \boldsymbol{C} & \mathbf{0}_{63} \\ \mathbf{0}_{36} & \mathbf{0}_{33} \end{bmatrix} + \boldsymbol{T}, \tag{4.1}$$

where $\mathbf{0}_{mn}$ denotes the $m \times n$ zero matrix; $\boldsymbol{C}$ is a 6×6 matrix of material tangent moduli whose components are given by

$$C_{IJ} = c_{ijkl}, \tag{4.2}$$

in which the relationships between the indices, namely, $I = I(i, j)$ and $J = J(k, l)$, are given by

I	i	j	J	k	l
1	1	1			
2	1	2			
3	2	2			
4	3	3			
5	2	3			
6	3	1			

(4.3)

and $\boldsymbol{T}$, the initial-stress matrix, is defined below:

$$
\boldsymbol{T} = \left[\begin{array}{cccccc|ccc}
\sigma_1 & \frac{\sigma_2}{2} & \cdot & \cdot & \cdot & \frac{\sigma_6}{2} & \frac{\sigma_2}{2} & \cdot & \frac{-\sigma_6}{2} \\
 & \frac{\sigma_1+\sigma_3}{4} & \frac{\sigma_2}{2} & \cdot & \frac{\sigma_6}{4} & \frac{\sigma_5}{4} & \frac{\sigma_3-\sigma_1}{4} & \frac{\sigma_6}{4} & \frac{-\sigma_5}{4} \\
 & & \sigma_3 & \cdot & \frac{\sigma_5}{2} & \cdot & \frac{-\sigma_2}{2} & \frac{\sigma_5}{2} & \cdot \\
\hline
 & & & \sigma_4 & \frac{\sigma_5}{2} & \frac{\sigma_6}{2} & \cdot & \frac{-\sigma_5}{2} & \frac{\sigma_6}{2} \\
 & & & & \frac{\sigma_3+\sigma_4}{4} & \frac{\sigma_2}{4} & \frac{-\sigma_6}{4} & \frac{\sigma_4-\sigma_3}{4} & \frac{\sigma_2}{4} \\
 & & & & & \frac{\sigma_4+\sigma_1}{4} & \frac{\sigma_5}{4} & \frac{-\sigma_2}{4} & \frac{\sigma_1-\sigma_4}{4} \\
\hline
 & & & & & & \frac{\sigma_1+\sigma_3}{4} & \frac{-\sigma_6}{4} & \frac{-\sigma_5}{4} \\
 & & \text{symm.} & & & & & \frac{\sigma_3+\sigma_4}{4} & \frac{-\sigma_2}{4} \\
 & & & & & & & & \frac{\sigma_4+\sigma_1}{4}
\end{array}\right], \tag{4.4}
$$

where

$$\sigma_I = \sigma_{ij}. \tag{4.5}$$

The $\boldsymbol{D}$ matrix is arranged to be compatible with the following ordering of strain and rotation components:

$$\gamma_{11}, 2\gamma_{12}, \gamma_{22}, \gamma_{33}, 2\gamma_{23}, 2\gamma_{31}, 2\omega_{12}, 2\omega_{23}, 2\omega_{31}. \tag{4.6}$$

The definition of $\boldsymbol{D}$ given above can be shown to be 'consistent', in the sense defined in [26], with a material response tensor defined by

$$\tilde{c}_{ijkl} = c_{ijkl} + \hat{c}_{ijkl}, \tag{4.7}$$

where

$$\hat{c}_{ijkl} = -\sigma_{ij}\delta_{kl} + (\sigma_{il}\delta_{jk} + \sigma_{jl}\delta_{ik} + \sigma_{ik}\delta_{jl} + \sigma_{jk}\delta_{il})/2. \tag{4.8}$$

The matrix form of the $\hat{c}_{ijkl}$'s is given by

$$\hat{\boldsymbol{C}} = \left[\begin{array}{ccc:ccc} \sigma_1 & \sigma_2 & -\sigma_1 & -\sigma_1 & 0 & \sigma_6 \\ 0 & \frac{\sigma_1+\sigma_3}{2} & 0 & -\sigma_2 & \frac{\sigma_6}{2} & \frac{\sigma_5}{2} \\ -\sigma_3 & \sigma_2 & \sigma_3 & -\sigma_3 & \sigma_5 & 0 \\ \hdashline -\sigma_4 & 0 & -\sigma_4 & \sigma_4 & \sigma_5 & \sigma_6 \\ -\sigma_5 & \frac{\sigma_6}{2} & 0 & 0 & \frac{\sigma_3+\sigma_4}{2} & \frac{\sigma_2}{2} \\ 0 & \frac{\sigma_5}{2} & -\sigma_6 & 0 & \frac{\sigma_2}{2} & \frac{\sigma_4+\sigma_1}{2} \end{array}\right]. \tag{4.9}$$

For additional details of the derivation, see [22].

4.1.1. Zero normal-stress projection

For application to shell analysis, the $\boldsymbol{D}$ matrix needs to be modified to account for the zero normal-stress condition. To this end, $\sigma_4 = \sigma_{33}$ is set to zero in $\boldsymbol{T}$ and a projection operator is constructed, as suggested by (3.18), to remove the row and column of $\boldsymbol{D}$ corresponding to γ_{33}, viz.

$$\tilde{\boldsymbol{D}} = \boldsymbol{P}^{\mathrm{t}}\boldsymbol{D}\boldsymbol{P}, \tag{4.10}$$

where

$$\boldsymbol{P} = \begin{bmatrix} \boldsymbol{p}_1 & \boldsymbol{p}_2 \\ \boldsymbol{0}_{35} & \boldsymbol{I}_3 \end{bmatrix}, \tag{4.11}$$

and

$$\boldsymbol{p}_1 = \left[\begin{array}{ccc:cc} 1 & 0 & 0 & 0 & 0 \\ 0 & 1 & 0 & 0 & 0 \\ 0 & 0 & 1 & 0 & 0 \\ \hdashline p_1 & p_2 & p_3 & p_5 & p_6 \\ 0 & 0 & 0 & 1 & 0 \\ 0 & 0 & 0 & 0 & 1 \end{array}\right], \qquad \boldsymbol{p}_2 = \left[\begin{array}{ccc} 0 & 0 & 0 \\ 0 & 0 & 0 \\ 0 & 0 & 0 \\ \hdashline 0 & p_7 & p_8 \\ 0 & 0 & 0 \\ 0 & 0 & 0 \end{array}\right]. \tag{4.12}$$

$\boldsymbol{I}_n$ is the $n \times n$ identity matrix, and

$$p_I = -\bar{C}_{4I}/\bar{C}_{44}, \quad I \leq 6, \qquad p_7 = \sigma_5/\bar{C}_{44}, \qquad p_8 = -\sigma_6/\bar{C}_{44}. \tag{4.13}$$

As may be seen, $\tilde{\boldsymbol{D}}$ is an 8×8 matrix. The matrix triple product in (4.10) may be efficiency implemented due to the simple, sparse structure of $\boldsymbol{P}$.

4.2. Strain–displacement matrix

In application to plates and shells, special treatment needs to be given to transverse shear terms to prevent a 'mesh-locking' phenomenon [23–25, 27, 35, 38, 44, 55]. A particularly effective treatment may be performed by employing the reduced/selective integration concept [25]. In the present formulation, we make use of an idea presented in [20, 21] which enables implementation of the selective integration procedure by a simple modification of the strain–displacement matrix. This technique has advantages in anisotropic and nonlinear situations, since it engenders only a minor change to the standard, element-array implementation.

The definition of the strain–displacement matrix adopted is given as follows:

$$\boldsymbol{B} = [\boldsymbol{B}_1, \boldsymbol{B}_2, \ldots, \boldsymbol{B}_{n_{en}}], \tag{4.14}$$

$$\boldsymbol{B}_a = \begin{bmatrix} \boldsymbol{B}_a^{\gamma} \\ \boldsymbol{B}_a^{\omega} \end{bmatrix}, \quad a = 1, 2, \ldots, n_{en}, \tag{4.15}$$

$$\boldsymbol{B}_a^{\gamma} = \left[\begin{array}{ccc:ccc} B_1 & 0 & 0 & B_4 & 0 & 0 \\ B_2 & B_1 & 0 & B_5 & B_4 & 0 \\ 0 & B_2 & 0 & 0 & B_5 & 0 \\ \hdashline 0 & \bar{B}_3 & \bar{B}_2 & 0 & \bar{B}_6 & \bar{B}_5 \\ \bar{B}_3 & 0 & \bar{B}_1 & \bar{B}_6 & 0 & \bar{B}_4 \end{array}\right], \tag{4.16}$$

$$\boldsymbol{B}_a^{\omega} = \left[\begin{array}{ccc:ccc} B_2 & -B_1 & 0 & B_5 & -B_4 & 0 \\ 0 & B_3 & -B_2 & 0 & B_6 & -B_5 \\ -B_3 & 0 & B_1 & -B_6 & 0 & B_4 \end{array}\right], \tag{4.17}$$

$$B_i = \begin{cases} N_{a,i} & i = 1, 2, 3, \\ (N_a z_a)_{,i-3}, & i = 4, 5, 6. \end{cases} \tag{4.18}$$

(Note that the derivatives in (4.18) are taken with respect to the lamina system at the point under consideration, e.g., $N_{a,i} = \partial N_a / \partial y_i^l$, where $\boldsymbol{y}^l = \boldsymbol{q}\boldsymbol{y}$.) The definition of the $\bar{B}_i$'s is considered below:

We assume a lamina quadrature rule is specified to integrate the element stiffness matrix and internal force vector. The quadrature points are the locations where the stresses and related data are stored. We wish to think of this rule as the 'normal' one for the element.

Another quadrature rule is introduced which may be thought of as a 'reduced' rule. For this rule, $\bar{n}_{\text{int}}$ and $\bar{\xi}_l$, $\bar{\eta}_l$ denote the number of points and locations, respectively. A special set of shape functions, $\bar{N}_l$'s, is defined with nodes at the quadrature points (i.e., $N_k(\bar{\xi}_l, \bar{\eta}_l) = \delta_{kl}$, $1 \le k, l \le \bar{n}_{\text{int}}$).

For example, if the element under consideration was a quadrilateral and the reduced rule was the 2×2 Gauss–Legendre rule, then the $\bar{N}_l$'s would be bilinear functions interpolating the 2×2 Gauss points.

The general form of the $\bar{B}_i$'s is given by

$$\bar{B}_i(\xi, \eta) = \sum_{I=1}^{\bar{n}_{\text{int}}} \bar{N}_I(\xi, \eta) B_i(\bar{\xi}_I, \bar{\eta}_I). \tag{4.19}$$

As an example, consider the 4-node bilinear quadrilateral. The normal rule is the 2×2 Gauss–Legendre rule. Take as the reduced rule the 1-point Gauss–Legendre rule, so that $\bar{n}_{\text{int}} = 1$, $\bar{N}_1 = 1$, and $\bar{\xi}_1 = \bar{\eta}_1 = 0$ (i.e., the element center). Then (4.19) reduces to

$$\bar{B}_i(\xi, \eta) = B_i(0, 0). \tag{4.20}$$

That is, the value at the center of the element is used to compute the transverse shear contribution.

REMARK 1. The row ordering of $\boldsymbol{B}_a$ is consistent with $\tilde{\boldsymbol{D}}$. The column ordering corresponds to $\Delta \bar{\boldsymbol{u}}_a^I$ followed by $\Delta \hat{\boldsymbol{U}}_a^I$, the increments in nodal displacement and nodal fiber displacement of the unit fiber vector, $\hat{\boldsymbol{Y}}_a^I$, respectively. In each case, the components are referred to the lamina basis at the point in question.

REMARK 2. A rational theory for including shear correction effects in the general nonlinear case does not appear to exist yet. There are several possible ways of going about this in the present formulation. An *ad hoc* procedure, which reduces to the usual one in the linear isotropic case and, at the same time, does not upset important symmetry properties in the general case, amounts to replacing each $\bar{B}_i$ in (4.16) by $\kappa^{1/2}\bar{B}_i$, where κ is the shear correction factor. (For the sample problems in section 7 we have employed $\kappa = 5/6$.) This must be done wherever the $\boldsymbol{B}$ matrix is employed. In this regard, we may mention strain increment evaluation and formulation of the element tangent stiffness and internal force (see section 4.4). Formally, strain increments may be computed as follows:

$$\boldsymbol{\gamma}_{\text{vec}} = \sum_{a=1}^{n_{en}} \boldsymbol{B}_a^{\gamma} \begin{bmatrix} \Delta \bar{\boldsymbol{u}}_a \\ \Delta \hat{\boldsymbol{U}}_a^I \end{bmatrix}, \tag{4.21}$$

where

$$\boldsymbol{\gamma}_{\text{vec}} = \begin{bmatrix} \gamma_1 \\ \gamma_2 \\ \gamma_3 \\ \gamma_5 \\ \gamma_6 \end{bmatrix} = \begin{bmatrix} \gamma_{11} \\ 2\gamma_{12} \\ \gamma_{22} \\ 2\gamma_{23} \\ 2\gamma_{31} \end{bmatrix}. \tag{4.22}$$

However, a more efficient procedure is to use the unmodified $\bar{B}_i$'s in (4.16) and simply replace γ_5 and γ_6 by $\kappa^{1/2}\gamma_5$ and $\kappa^{1/2}\gamma_6$, respectively.

We wish to emphasize that the preceding ideas are tentative and will likely undergo revision upon the appearance of a theory of shear-correction effects in nonlinear analysis.

4.3. Transformation matrices

Two matrices are required to transform element arrays to global degrees-of-freedom. In the present formulation we allow a choice of global rotational degrees of freedom.

The first is $\Delta\hat{U}$ (i.e., the three components of the fiber displacement with respect to the global coordinate system). This case appears to be advantageous when beam-like stiffeners are present in that the identical degrees of freedom are convenient for use with beams.

The second choice of global rotational degrees-of-freedom is $\Delta\theta_1$ and $\Delta\theta_2$, the canonical rotation increments defined with respect to the nodal fiber coordinate system. For this choice, rank-deficiency problems emanating from the in-plane torsional mode are obviated without recourse to artificial devices (see [30] for background).

The choice of nodal rotational degrees of freedom may be made on a node-by-node basis. In either case, the nodal displacement increment degrees-of-freedom are taken to be the components with respect to the global coordinate system. For the first choice there are six degrees of freedom per node, whereas in the second there are five.

The required arrays are given as follows:

$$\boldsymbol{Q}_a = \begin{cases} \begin{bmatrix} \boldsymbol{q} & \boldsymbol{0}_{33} \\ \boldsymbol{0}_{33} & \boldsymbol{q} \end{bmatrix} & 6 \text{ dof}, \\ \begin{bmatrix} \boldsymbol{q} & \boldsymbol{0}_{32} \\ \boldsymbol{0}_{33} & \bar{\boldsymbol{r}}_a \end{bmatrix} & 5 \text{ dof}, \end{cases} \tag{4.23}$$

$$\bar{\boldsymbol{r}}_a = \boldsymbol{r}_a \begin{bmatrix} -1 & 0 \\ 0 & -1 \\ 0 & 0 \end{bmatrix}, \tag{4.24}$$

$$\boldsymbol{S}_a = \begin{cases} \boldsymbol{I}_6 & 6 \text{ dof}, \\ \begin{bmatrix} \boldsymbol{I}_3 & \boldsymbol{0}_{32} \\ \boldsymbol{0}_{33} & \bar{\boldsymbol{s}}_a \end{bmatrix} & 5 \text{ dof}, \end{cases} \tag{4.25}$$

$$\bar{\boldsymbol{s}}_a = \boldsymbol{s}_a \begin{bmatrix} -1 & 0 \\ 0 & -1 \\ 0 & 0 \end{bmatrix}. \tag{4.26}$$

4.4. Tangent stiffness matrix and internal force vector

The element stiffness and internal force are defined as follows:

$$\boldsymbol{k} = [\boldsymbol{k}_{ab}], \qquad \boldsymbol{f}^{\text{int}} = \{\boldsymbol{f}_a^{\text{int}}\}, \tag{4.27}$$

$$\boldsymbol{k}_{ab} = \int_{\square}\int_{-1}^{+1} \boldsymbol{Q}_a^{\text{t}} \boldsymbol{B}_a^{\text{t}} \tilde{\boldsymbol{D}} \boldsymbol{B}_b \boldsymbol{Q}_{bj} \, \mathrm{d}\zeta \, \mathrm{d}\square, \tag{4.28}$$

$$\boldsymbol{f}_a^{\text{int}} = \int_{\square}\int_{-1}^{+1} \boldsymbol{Q}_a^{\text{t}} (\boldsymbol{B}_a^{\gamma})^{\text{t}} \boldsymbol{\sigma}_{\text{vec}j} \, \mathrm{d}\zeta \, \mathrm{d}\square, \tag{4.29}$$

where

$$\int_{\square} \cdots \mathrm{d}\square = \int_{-1}^{+1}\int_{-1}^{+1} \cdots \mathrm{d}\xi\,\mathrm{d}\eta \quad \text{(lamina integral)}, \tag{4.30}$$

$$j = \det \begin{bmatrix} y_{1,\xi} & y_{1,\eta} & y_{1,\zeta} \\ y_{2,\xi} & y_{2,\eta} & y_{2,\zeta} \\ y_{3,\xi} & y_{3,\eta} & y_{3,\zeta} \end{bmatrix}, \tag{4.31}$$

$$\boldsymbol{\sigma}_{\mathrm{vec}} = \begin{bmatrix} \sigma_1 \\ \sigma_2 \\ \sigma_3 \\ \sigma_5 \\ \sigma_6 \end{bmatrix} = \begin{bmatrix} \sigma_{11} \\ \sigma_{12} \\ \sigma_{22} \\ \sigma_{23} \\ \sigma_{31} \end{bmatrix}. \tag{4.32}$$

REMARK 1. In most situations the variation of $\boldsymbol{Q}_a$ with ζ will be insignificant. For this reason we have adopted the approximation $Q_a(\zeta) \simeq Q_a(\bar{\zeta})$ which enables $\boldsymbol{Q}_a$ to be removed from the fiber integral, viz.

$$\boldsymbol{k}_{ab} = \int_{\square} \boldsymbol{Q}_a^{\mathrm{t}} \left[\int_{-1}^{+1} \boldsymbol{B}_a^{\mathrm{t}} \tilde{\boldsymbol{D}} \boldsymbol{B}_b j \,\mathrm{d}\zeta \right] \boldsymbol{Q}_b \,\mathrm{d}\square \tag{4.33}$$

$$\boldsymbol{f}_a^{\mathrm{int}} = \int_{\square} \boldsymbol{Q}_a^{\mathrm{t}} \left[\int_{-1}^{+1} (\boldsymbol{B}_a^{\gamma})^{\mathrm{t}} \boldsymbol{\sigma}_{\mathrm{vec}} j \,\mathrm{d}\zeta \right] \mathrm{d}\square. \tag{4.34}$$

REMARK 2. When effects due to the initial stress matrix, $\boldsymbol{T}$, may be neglected, the calculation of the tangent stiffness simplifies considerably. In this case the $\boldsymbol{B}_a^{\mathrm{t}} \tilde{\boldsymbol{D}} \boldsymbol{B}_b$ product may be replaced by $(\boldsymbol{B}_a^{\gamma})^{\mathrm{t}} \tilde{\boldsymbol{C}} \boldsymbol{B}_b^{\gamma}$, where

$$\tilde{\boldsymbol{C}} = \boldsymbol{p}_1^{\mathrm{t}} \boldsymbol{C} \boldsymbol{p}_1. \tag{4.35}$$

Note that $\tilde{\boldsymbol{C}}$ is a 5×5 matrix.

4.5. External force vector

We allow for both body and surface force vectors.

4.5.1. Body force

The element body force vector is given by

$$\boldsymbol{f}^{\mathrm{body}} = \{\boldsymbol{f}_a^{\mathrm{body}}\}, \tag{4.36}$$

$$\boldsymbol{f}_a^{\mathrm{body}} = \boldsymbol{S}_a^{\mathrm{t}} \int_{\square}\int_{-1}^{+1} \boldsymbol{N}_a^{\mathrm{t}} \boldsymbol{b} \rho_0 j_0 \,\mathrm{d}\zeta \,\mathrm{d}\square, \tag{4.37}$$

where ρ_0 is the mass density in the initial configuration, $\boldsymbol{b}$ is the prescribed body force vector (per unit mass),

$$j_0 = \begin{bmatrix} x_{1,\xi} & x_{1,\eta} & x_{1,\zeta} \\ x_{2,\xi} & x_{2,\eta} & x_{2,\zeta} \\ x_{3,\xi} & x_{3,\eta} & x_{3,\zeta} \end{bmatrix} \tag{4.38}$$

and

$$\boldsymbol{N}_a = \left[\begin{array}{ccc|ccc} N_a & 0 & 0 & N_a z_a & 0 & 0 \\ 0 & N_a & 0 & 0 & N_a z_a & 0 \\ 0 & 0 & N_a & 0 & 0 & N_a z_a \end{array}\right]. \tag{4.39}$$

4.5.2. Surface force

The element surface force vector is defined by

$$\boldsymbol{f}^{\text{surf}} = \{\boldsymbol{f}_a^{\text{surf}}\}, \tag{4.40}$$

$$\boldsymbol{f}_a^{\text{surf}} = \boldsymbol{S}_a^{\text{t}} \int_{\square} \boldsymbol{N}_a^{\text{t}} \boldsymbol{h} j_s \, \mathrm{d}\square, \qquad \zeta = \begin{cases} +1 & \text{top} \\ -1 & \text{bottom,} \end{cases} \tag{4.41}$$

$$j_s = \|\boldsymbol{y}_{,\xi} \times \boldsymbol{y}_{,\eta}\| \quad \text{surface jacobian,} \tag{4.42}$$

where $\boldsymbol{h}$ is the surface force vector (per unit surface area).

It is convenient to allow for pressure and shear surface force vectors as separate cases:

4.5.3. Pressure

In this case

$$\boldsymbol{h} = (-1)^{\zeta} p \boldsymbol{n}, \tag{4.43}$$

$$\boldsymbol{n} = (\boldsymbol{y}_{,\xi} \times \boldsymbol{y}_{,\eta})/\|\boldsymbol{y}_{,\xi} \times \boldsymbol{y}_{,\eta}\|, \tag{4.44}$$

where p is the pressure and $\boldsymbol{n}$ is the unit normal vector to the surface.

4.5.4. Shear

We assume that the shear is specified in the ξ and/or η directions on the surface in question. In this case the surface force vector is given by

$$\boldsymbol{h} = h_\xi \boldsymbol{y}_{,\xi}/\|\boldsymbol{y}_{,\xi}\| + h_\eta \boldsymbol{y}_{,\eta}/\|\boldsymbol{y}_{,\eta}\|, \tag{4.45}$$

where h_ξ and h_η are the shears in the ξ and η directions, respectively.

The element external force vector is defined by

$$\boldsymbol{f}^{\text{ext}} = \boldsymbol{f}^{\text{body}} + \boldsymbol{f}^{\text{surf}}. \tag{4.46}$$

The element out-of-balance force, or residual, is given by

$$\Delta \boldsymbol{f} = \boldsymbol{f}^{\text{ext}} - \boldsymbol{f}^{\text{int}}. \tag{4.47}$$

4.6. Fiber numerical integration

In the general nonlinear case, fiber integrals need be evaluated by a numerical integration technique. Several ways of going about this present themselves, each having advantages in certain circumstances.

If the integrand is a smooth function of ζ (e.g., when the shell consists of one homogeneous, elastic layer), then Gaussian quadrature is most efficient. If the reference surface is taken to be the midsurface, then the 1-point Gauss rule (i.e., midpoint rule) only senses membrane effects. At least two points are required to manifest the bending behavior.

If it is desired to include the outermost fiber points (i.e., $\zeta = \pm 1$) in the evaluation, then the Lobatto rules are most accurate for smooth integrands. The 2-point, trapezoidal rule and 3-point, Simpson's rule are the first two members of the Lobatto family.

If the shell is built up from a series of layers of different materials such that the material properties and stresses are discontinuous functions of ζ, then Gaussian rules may be effectively used over each layer. If there are a large number of approximately equal-sized layers, then the midpoint rule on each layer should suffice. If, on the other hand, there are a small number of layers, or if the layers vary considerably in thickness, then different Gaussian rules should be assigned to individual layers. This is facilitated in our formulation by allowing the user to input the location and weights of the fiber quadrature rule. Thus any special set of circumstances may be accommodated.

4.7. Stress resultants

Bending moments, membrane forces, and transverse shear resultants may be computed at the lamina quadrature points of the 'normal' rule (see section 4.2) at which stresses are stored. Let $\tilde{\boldsymbol{\xi}}_l = (\tilde{\xi}_l, \tilde{\eta}_l)$, $1 \le l \le n_{\text{int}}$, denote the quadrature points of the normal rule.

4.7.1. Moments

The moments may be calculated from the following expression:

$$m_{\alpha\beta}(\tilde{\boldsymbol{\xi}}_l) = \int_{-1}^{+1} \sigma_{\alpha\beta}(\tilde{\boldsymbol{\xi}}_l, \zeta) z(\tilde{\boldsymbol{\xi}}_l, \zeta)\, \mathrm{d}\zeta\, z_{,\zeta}(\tilde{\boldsymbol{\xi}}_l), \quad 1 \le \alpha, \beta \le 2, \tag{4.48}$$

$$z(\tilde{\boldsymbol{\xi}}_l, \zeta) = N_+(\zeta) z^+(\tilde{\boldsymbol{\xi}}_l) + N_-(\zeta) z^-(\tilde{\boldsymbol{\xi}}_l), \tag{4.49}$$

$$z^{\pm}(\tilde{\boldsymbol{\xi}}_l) = \sum_{a=1}^{n_{en}} N_a(\tilde{\boldsymbol{\xi}}_l) z_a^{\pm}, \tag{4.50}$$

$$z_{,\zeta}(\tilde{\boldsymbol{\xi}}_l) = [z^+(\tilde{\boldsymbol{\xi}}_l) - z^-(\tilde{\boldsymbol{\xi}}_l)]/2. \tag{4.51}$$

4.7.2. Membrane forces

The membrane forces may be computed as follows:

$$n_{\alpha\beta}(\tilde{\boldsymbol{\xi}}_l) = \int_{-1}^{+1} \sigma_{\alpha\beta}(\tilde{\boldsymbol{\xi}}_l, \zeta)\, \mathrm{d}\zeta\, z_{,\zeta}(\tilde{\boldsymbol{\xi}}_l), \quad 1 \le \alpha, \beta \le 2. \tag{4.52}$$

4.7.3. Shears

The shears may be computed from the following formula:

$$q_\alpha(\bar{\xi}_l) = \kappa^{1/2} \int_{-1}^{+1} \sigma_{\alpha 3}(\bar{\xi}_l, \zeta)\, \mathrm{d}\zeta\, z_{,\zeta}(\bar{\xi}_l). \tag{4.53}$$

Stresses are stored at ζ-locations corresponding to the quadrature points of the fiber rule, and the integrations of (4.48), (4.52) and (4.53) are performed using these rules. Stresses and stress resultants may be defined at other points in the elements by employing various interpolation, extrapolation, and smoothing schemes.

The sign conventions for the stress resultants are illustrated in fig. 9.

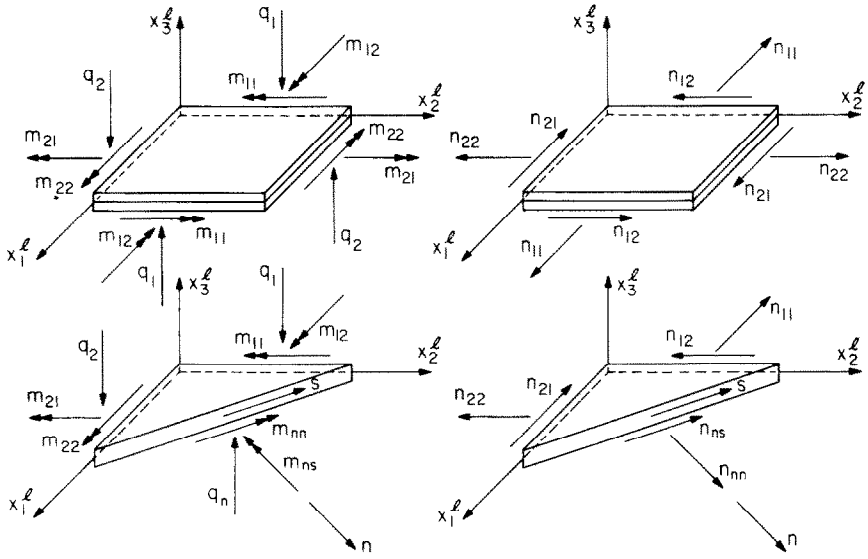

Fig. 9. Sign conventions for stress resultants

4.8. Boundary conditions

It may be simply verified that the following represent correct conjugate quantities which may be specified along boundaries:

kinematic $\leftrightarrow$ mechanical

$$\bar{\boldsymbol{u}} \qquad \boldsymbol{F} = \int_{-1}^{+1} \boldsymbol{\hbar}\, \mathrm{d}\zeta\, z_{,\zeta} \tag{4.54}$$

$$\hat{\boldsymbol{U}} \qquad \boldsymbol{M} = \int_{-1}^{+1} \boldsymbol{\hbar} z\, \mathrm{d}\zeta\, z_{,\zeta}. \tag{4.55}$$

In the above, $\boldsymbol{\hbar}$ is interpreted as the traction vector along the edge surface. Thus $\boldsymbol{F}$ is the edge force vector (per unit length) and $\boldsymbol{M}$ is the edge moment vector (per unit length). The

kinematic counterparts are $\bar{u}$, the reference surface displacement vector, and $\hat{U}$ the displacement of the unit vector which defines the orientation of the fiber. Note that M is nonzero even for constant $\hbar$ when the reference surface is not taken to be the midsurface.

Note that nodal moments need be transformed to the fiber system when the five degree-of-freedom nodal system is adopted. This is achieved by premultiplication by $\bar{s}_a^t$ (see section 4.3) which is most conveniently handled by automation on a global nodal basis.

5. Global matrix equations

The global matrix equations may be formulated from the element arrays as follows:

$$K\Delta d = \Delta F, \tag{5.1}$$

$$K = \mathop{\mathbf{A}}_{e=1}^{n_{el}} (k^e) \qquad \text{tangent stiffness,} \tag{5.2}$$

$$\Delta F = \mathop{\mathbf{A}}_{e=1}^{n_{el}} (\Delta f^e) \qquad \text{out-of-balance force,} \tag{5.3}$$

where Δd is the global generalized displacement-increment vector; $\mathbf{A}$ is the finite element assembly operator which assigns element entries to the appropriate locations of the global arrays, and which accounts for the effects of kinematic boundary conditions; n_{el} is the number of elements; and k^e and Δf^e are the eth-element tangent stiffness and out-of-balance force. (5.1) is used in an iterative/incremental Newton–Raphson format to obtain solutions to the boundary-value problem under consideration.

6. Shell elements

The elements employed in the present work are generalizations of ones used in our research on plate bending [23–25, 27].

6.1. Reduced integration Lagrange elements

The lamina shape functions and quadrature rules for the Lagrange elements are shown in fig. 10. In each case the appropriate reduced rule is one order lower than the normal rule. If the normal rule and reduced rule are combined, as described in section 4.2, the element is called a 'selective integration element'. If either the normal or reduced rule is used exclusively [i.e., if $\bar{B}_i \equiv B_i$ in (4.16)], then the element is called a 'uniform integration element'. Uniform normal integration tends to cause elements to 'lock' in thin shell applications. This phenomenon is especially pronounced for low-order elements. On the other hand, selective and uniform reduced integration elements behave well in thin shell applications, but may occasionally engender rank deficiency (i.e., spurious 'mechanisms'). The problem is less acute for the selective integration elements than for the uniform reduced integration elements. In most situations, the mechanisms are precluded from globally forming by boundary conditions,

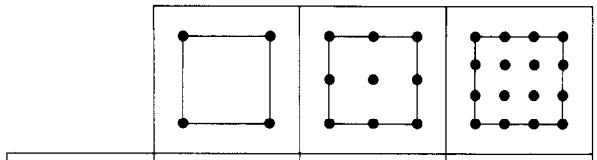

lamina shape functions	bilinear	biquadratic	bicubic
normal Gaussian rule	2 × 2	3 × 3	4 × 4
reduced Gaussian rule	1 × 1	2 × 2	3 × 3

Fig. 10. Lagrange shell elements.

but nevertheless represent a potentially dangerous deficiency. For background information on this problem and other relevant material, the interested reader is urged to consult [25].

Research has been undertaken to efficiently remove the mechanisms. One successful procedure is described next.

6.2. *Heterosis elements*

The heterosis concept was originally developed in [23] to eliminate the spurious zero-energy mode in the 9-node, selectively integrated Lagrange element. The resulting element possesses correct rank and behaves well in the thin shell limit. The concept may be generalized to higher-order elements [24].

Implementation of the heterosis element begins by constructing the arrays for the selectively integrated Lagrange element (say, e.g., $\boldsymbol{k}_{\text{Lag}}$, $\Delta \boldsymbol{f}_{\text{Lag}}$, etc.). Then a projection matrix, $\boldsymbol{H}$, is constructed from the serendipity shape functions associated with the element-boundary nodes. The role $\boldsymbol{H}$ plays is to eliminate all translational degrees of freedom from the internal (i.e., nonboundary) nodes by restraining them to interpolate the serendipity shape functions (see [24] for additional details). The heterosis arrays are then defined by

$$\boldsymbol{k}_{\text{het}} = \boldsymbol{H}^{\text{t}} \boldsymbol{k}_{\text{Lag}} \boldsymbol{H}, \tag{6.1}$$

$$\Delta \boldsymbol{f}_{\text{het}} = \boldsymbol{H}^{\text{t}} \Delta \boldsymbol{f}_{\text{Lag}}. \tag{6.2}$$

At this point, if desired, the internal rotational degrees of freedom may be removed by static condensation.

7. Sample problems

All computations were performed on an IBM 3032 computer at the California Institute of Technology Computer Center in double precision (64 bits per floating-point word).

The following elements were studied herein:

Lagrange elements

U1—4-node, uniform reduced integration.
S1—4-node, selective reduced integration.
S2—9-node, selective reduced integration.

We also considered the heterosis element, HS2, which is a modification of S2; see section 6.2.

Our interest in U1 stems from its potential use in the so-called 'hydrocodes' [18]. Here, economy is a prime concern and U1, despite serious rank-deficiency problems, holds promise of being the basis of optimally economical shell analysis procedures. Economy and simplicity have prompted several shell element developments in recent years (see, e.g., [5, 7, 13, 17, 19, 29, 30, 34, 47, 53]).

We employed both the full definition of the rotation matrix $\boldsymbol{R}$, see (3.16), and the corotational approximation $\boldsymbol{R} \simeq \boldsymbol{I}$. In no case were the differences discernible, which is not surprising since the problems considered may be classified as small strain, large rotation ones.

The material model is considered to be homogeneous and linearly elastic in the sense that the c_{ijkl}'s are taken to be

$$c_{ijkl} = \lambda \delta_{ij}\delta_{kl} + \mu(\delta_{ik}\delta_{jl} + \delta_{il}\delta_{jk}), \tag{7.1}$$

where λ and μ are the Lamé parameters.

The fiber integration was performed using the 2-point Gauss rule. Higher-order Gauss rules were experimented with, but for the cases considered they produced no discernible differences.

The shear correction factor, κ, was taken to be 5/6 throughout, and the five degree-of-freedom nodal system was employed in each case.

7.1. Plate strip under uniform load

This problem is actually one-dimensional and an analytical solution is available in Timoshenko and Woinowsky-Krieger [48]. The plate is considered to be of infinite extent and is simply supported. Thus we may view the configuration as a simply-supported beam in which a plane strain condition is maintained perpendicular to the plane of deformation. In our calculations we employed a mesh of five 4-node elements for half of the beam and restrained all out-of-plane degrees-of-freedom. Pertinent data and results are shown in fig. 11. The load was treated as nonconservative. Comparison is made with the analytical solution and results of Horrigmoe [19] who employed hybrid elements. Both S1 and U1 elements yielded virtually identical results for this case. The S1 elements took approximately 2 iterations per load step, whereas the U1 elements took 4 to 5. Nevertheless, CPU time for the S1 elements was more than double that for the U1 elements. For small problems of this type, all other things being equal, the CPU time is dominated by the number of numerical integration points.

7.2. Shallow circular arch under concentrated load

The problem statement is depicted in fig. 12. This problem is also one-dimensional and has

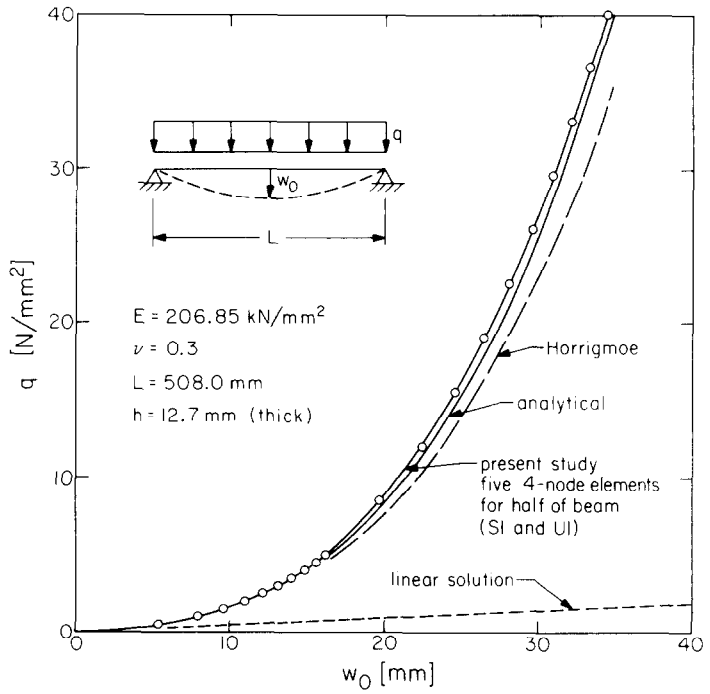

Fig. 11. Plate strip under uniform load.

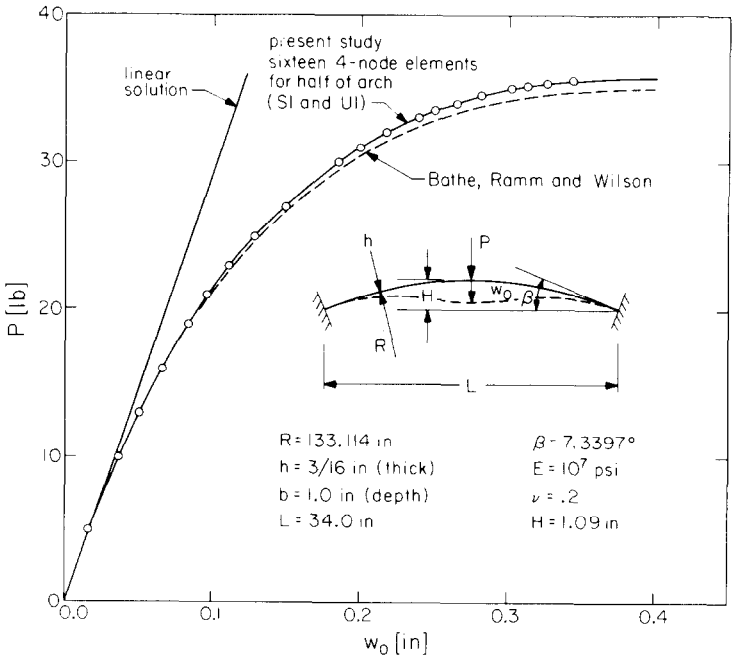

Fig. 12. Shallow circular arch under concentrated load.

been solved previously by Bathe et al. [9] using 8-node continuum elements. The results in the present study were obtained using sixteen 4-node elements for half the arch. Out-of-plane degrees-of-freedom were set to zero. As in the previous analysis, the results for S1 and U1 elements were virtually identical. In each case snap-through occurred at $P = 35.8$ lb. The number of iterations per step was 1 to 2 for the S1 elements and averaged slightly over 4 per step for the U1 elements. Again, however, the S1 analysis required more than double the CPU time of the U1 analysis.

7.3. Clamped square plate under uniform load

The problem configuration is defined in fig. 13. Plotted results are for four HS2 elements and sixteen U1 elements. We also used meshes of four S2 elements, and sixteen and sixty-four S1 elements. In the latter three cases, the results fell pointwise between the former two plotted cases. For clarity, the latter three cases were omitted from the plotted results. Comparison is made with the finite element results of Kawai and Yoshimura [31] and the classical Rayleigh–Ritz solution obtained by Way [50].

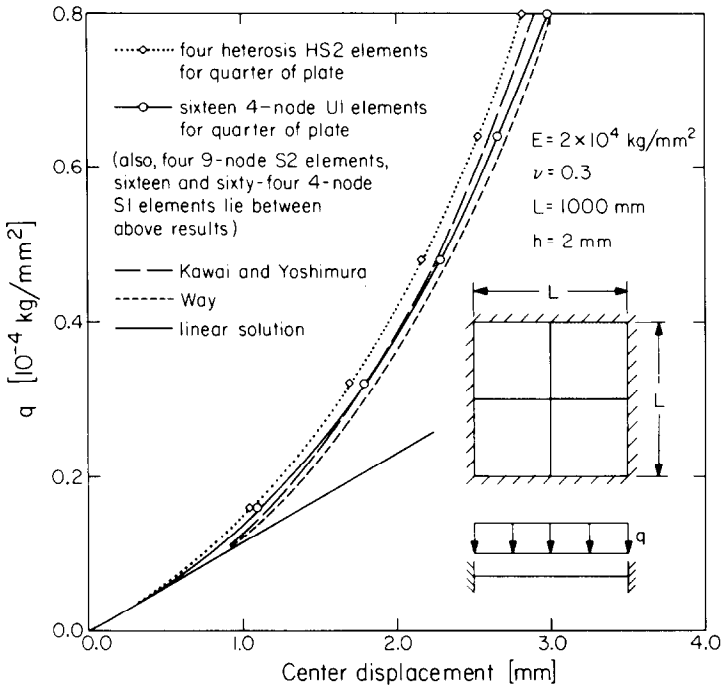

Fig. 13. Clamped square plate under uniform load.

For this problem we experimented with omitting the $\boldsymbol{T}$ and $\hat{\boldsymbol{C}}$ matrices in the calculations. We found that this increased the number of iterations per load step from an average of 3 when we included both $\boldsymbol{T}$ and $\hat{\boldsymbol{C}}$, to about 7 or 8. We also experimented with treating the loading as conservative and nonconservative. This produced no discernible differences.

7.4. Hinged cylindrical shell under concentrated load

This problem is illustrated in fig. 14. We employed sixteen-element meshes of S1 and U1 elements, and four-element meshes of S2 and HS2 elements. Due to symmetry, only one-quarter of the shell had to be modelled. All of our results were in close agreement and could not be distinguished on the scale of the plot. Comparison is made with results obtained by Horrigmoe [19] and Bathe and Bolourchi [8].

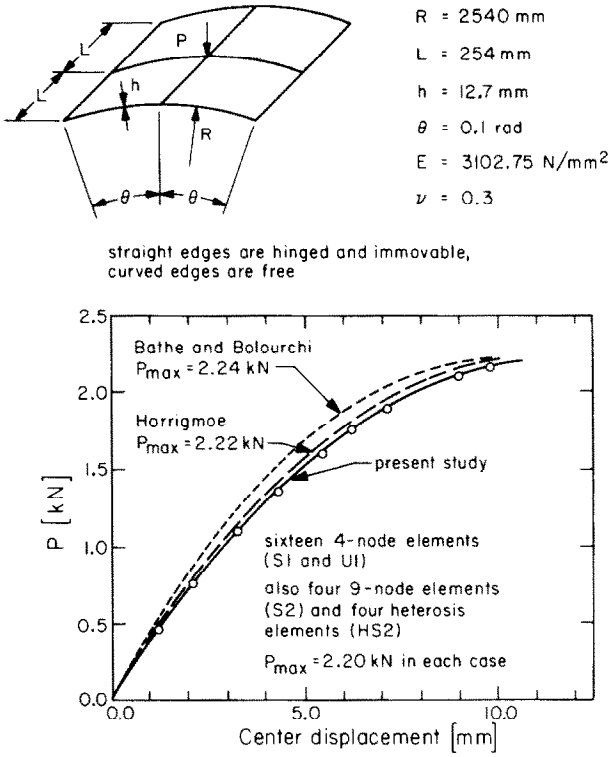

Fig. 14. Hinged cylindrical shell under concentrated load.

8. Conclusions

In the present work we have described a general three-dimensional finite element formulation for quasistatic nonlinear shell analysis. The theory presented herein represents an extension to the nonlinear regime of several works of the senior author and colleagues on linear plates and shells. Noteworthy features of the present formulation are: the extension of the selective integration procedure to the fully-coupled nonlinear case which, in particular, facilitates the development of a nonlinear heterosis-type shell element; presentation of a constitutive algorithm which is 'incrementally objective' for large rotation increments, maintains the zero normal-stress condition in the rotating lamina referential frame for a given three-dimensional constitutive equation, sheds light on the 'corotational hypothesis' and enables its use for arbitrary higher-order elements; and a simple treatment of finite nodal

rotations which precludes the appearance of unstabilized, in-plane rotational modes. Numerical examples indicate the good behavior of the elements studied.

Nevertheless, the development of optimal element procedures for general nonlinear shell analysis is far from a reality, and much additional research is needed. Particular subjects which warrant further study are: the correction of zero-energy modes which still afflict some of the elements; a theory of shear-correction factors for nonlinear analysis; a clean generalization of procedures described in [27, 34, 42] to stabilize the thin-shell limit in short word-length calculations; methods for improving the behavior of elements, especially low-order ones, when highly distorted; a serious investigation of the accuracy of shear resultants, which are important in many practical engineering situations; extension to dynamics; and more extensive numerical correlation studies into problems involving post-buckling phenomena.

Acknowledgments

We wish to gratefully acknowledge the following individuals and organizations for their interest and support of the research presented herein: J. Crawford, Civil Engineering Laboratory, Port Hueneme, California; the Electric Power Research Institute, Palo Alto, CA; and the National Science Foundation.

Appendix A. Reduced integration of membrane effects

After completion of the problem solving portion of the present work, we became aware of the paper by Parisch [42]. In this work, among other things, it is argued that it is very important to also underintegrate the membrane portion of the stiffness for the 9-node Lagrange element. Similar arguments have been previously made by MacNeal [34] in the context of the 4-node element. MacNeal urges a special selective treatment for this purpose. In the numerical studies presented herein we obtained good results without reduced integration of membrane effects, but according to MacNeal and Parisch, significant improvements will be noted in many circumstances, so it is worthwhile to consider how these modifications may be incorporated in the present formulation. In fact, the modifications are trivially included by slight changes to the definition of the membrane portion of the matrix $\boldsymbol{B}_a^\gamma$ originally defined in (4.16).

Uniform reduced integration of membrane effects

In this case

$$\boldsymbol{B}_a^\gamma = \left[\begin{array}{ccc:c} \bar{\boldsymbol{B}}_1 & 0 & 0 & \text{other} \\ \bar{\boldsymbol{B}}_2 & \bar{\boldsymbol{B}}_1 & 0 & \text{terms} \\ 0 & \bar{\boldsymbol{B}}_2 & 0 & \text{identical} \\ \hdashline & & & \text{to (4.16)} \end{array}\right]. \tag{A.1}$$

Selective reduced integration of membrane effects

In this case, only the shear-strain term is underintegrated:

$$\boldsymbol{B}_a^{\gamma} = \left[\begin{array}{ccc|c} B_1 & 0 & 0 & \text{other} \\ \bar{B}_2 & \bar{B}_1 & 0 & \text{terms} \\ 0 & B_2 & 0 & \text{identical} \\ \hline & & & \text{to (4.16)} \end{array}\right]. \tag{A.2}$$

Note that there is no 'invariance' problem in this case, since the entries of $\boldsymbol{B}_a^{\gamma}$ are defined with respect to lamina coordinates which in turn are defined intrinsically by the element geometry.

There are several other important ideas which are treated in the papers of MacNeal and Parisch, and these will be brought to bear on the present formulation in future works.

References

[1] S. Ahmad, B.M. Irons and O.C. Zienkiewicz, Analysis of thick and thin shell structures by curved finite elements, Internat. J. Numer. Meths. Engrg. 2 (1970) 419–451.

[2] J.H. Argyris, Recent advances in matrix methods of structural analysis, Progress in Aeronautical Sciences, Vol. 4 (Pergamon Press, Oxford, 1964).

[3] J.H. Argyris, Continua and discontinua, Proc. of the Conference on Matrix Methods in Structural Mechanics, Wright-Patterson Air Force Base, Ohio, October 1965.

[4] J.H. Argyris, H. Balmer, J.St. Doltsinis, P.C. Dunne, M. Haase, M. Kleiber, G.A. Malejannakis, H.-P. Mlejnek, M. Müller and D.W. Scharpf, Finite element method—the natural approach, Comput. Meths. Appl. Mech. Engrg. 17/18 (1979) 1–106.

[5] J.H. Argyris and P.C. Dunne, Post-buckling, finite element analysis of circular cylinders under end load, Report No. 224, Institut für Statik und Dynamik der Luft- und Raumfahrtkonstruktionen, University of Stuttgart, Germany (1977).

[6] J.H. Argyris, P.C. Dunne, G.A. Malejannakis and D.W. Scharpf, On large displacement—small strain analysis of structures with rotational degrees of freedom, Comput. Meths. Appl. Mech. Engrg. 14 (1978) 401–451; 15 (1978) 99–135.

[7] J.H. Argyris, P.C. Dunne, G.A. Malejannakis and E. Schelkle, A simple triangular facet shell element with applications to linear and nonlinear equilibrium and elastic stability problems, Comput. Meths. Appl. Mech. Engrg. 10 (1977) 371–403; 11 (1977) 97–131.

[8] K.J. Bathe and S. Bolourchi, A geometric and material nonlinear plate and shell element, J. Comput. Struct., to appear.

[9] K.J. Bathe, E. Ramm and E.L. Wilson, Finite element formulations for large displacement and large strain analysis, Report UC-SESM 73-14, Department of Civil Engineering, University of California, Berkeley (September 1973).

[10] T. Belytschko and L. Glaum, Applications of higher-order corotational formulations for nonlinear finite element analysis, Comput. and Struct. 10 (1979) 175–182.

[11] T. Belytschko and B.J. Hsieh, Nonlinear transient finite element analysis with convected coordinates, Internat. J. Numer. Meths. Engrg. 7 (1973) 255–271.

[12] T. Belytschko, L. Schwer and M.J. Klein, Large displacement transient analysis of space frames, Internat. J. Numer. Meths. Engrg. 11 (1977) 64–84.

[13] M. Berkovic, Thin shell isoparametric elements, Proc. Second World Congress on Finite Element Methods, Bournemouth, Dorset, England, October 1978.

[14] B. Brendel and E. Ramm, Linear and nonlinear stability analysis of cylindrical shells, Internat. Conf. on Engineering Application of the Finite Element Method, Høvik, Norway, May 9–11, 1979.

[15] R.H. Gallagher, Finite Element Analysis Fundamentals (Prentice-Hall, Englewood Cliffs, NJ, 1975).

[16] R.H. Gallagher, Shell elements, Proc. First World Congress on Finite Element Methods in Structural Mechanics, Bournemouth, England, 1975.

[17] G.L. Goudreau, A computer module for one step dynamic response of an axisymmetric plane linear elastic thin shell, Lawrence Livermore Laboratory Report No. UCID-17730 (February 1978).

[18] G.L. Goudreau and J.O. Hallquist, Synthesis of hydrocode and finite element technology for large deformation Lagrangian computation, Preprints of the 5th International Seminar on Computational Aspects of the Finite Element Method, Berlin (West), Germany, August 20–21, 1979.
[19] G. Horrigmoe, Finite element instability analysis of free-form shells, Report 77-2, Division of Structural Mechanics, Norwegian Institute of Technology, University of Trondheim, Norway (May 1977).
[20] T.J.R. Hughes, Recent developments in computer methods for structural analysis, Nucl. Engrg. Des. 57(2) (1980) 427–439.
[21] T.J.R. Hughes, Generalization of selective integration procedures to anisotropic and nonlinear media, Internat. J. Numer. Meths. Engrg. 15 (1980) 1413–1418.
[22] T.J.R. Hughes, On consistently derived tangent stiffness matrices, in preparation.
[23] T.J.R. Hughes and M. Cohen, The 'heterosis' finite element for plate bending, Comput. and Struct. 9 (1978) 445–450.
[24] T.J.R. Hughes and M. Cohen, The 'heterosis' family of plate finite elements, Proc. ASCE Electronic Computations Conference, St. Louis, MO, August 6–8, 1979.
[25] T.J.R. Hughes, M. Cohen and M. Haroun, Reduced and selective integration techniques in the finite element analysis of plates, Nucl. Engrg. Des. 46(1) (1978) 203–222.
[26] T.J.R. Hughes and K.S. Pister, Consistent linearization in mechanics of solids and structures, Comput. and Struct. 8 (1978) 391–398.
[27] T.J.R. Hughes, R.L. Taylor and W. Kanoknukulchai, A simple and efficient element for plate bending, Internat. J. Numer. Meths. Engrg. 11(10) (1977) 1529–1543.
[28] T.J.R. Hughes and J. Winget, Finite rotation effects in numerical integration of rate constitutive equations arising in large-deformation analysis, Internat. J. Numer. Meths. Engrg. 15 (1980) 1862–1867.
[29] W. Kanoknukulchai, A large deformation formulation for shell analysis by the finite element method, Ph.D. Thesis, University of California, Berkeley, November 1978.
[30] W. Kanoknukulchai, A simple and efficient finite element for general shell analysis, Internat. J. Numer. Meths. Engrg. 14 (1979) 179–200.
[31] T. Kawai and N. Yoshimura, Analysis of large deflection of plates by the finite element method, Internat. J. Numer. Meths. Engrg. 1 (1969) 123–133.
[32] R.D. Krieg and S.W. Key, Implementation of a time independent plasticity theory into structural computer programs, Constitutive equations in viscoplasticity: computational and engineering aspects, AMD Vol. 20 (ASME, New York, 1976).
[33] R.D. Krieg and D.B. Krieg, Accuracies of numerical solution methods for the elastic-perfectly plastic model, J. Pressure Vessel Technol. (November 1977) 510–515.
[34] R.H. MacNeal, A simple quadrilateral shell element, Comput. and Struct. 8 (1978) 175–183.
[35] D.S. Malkus and T.J.R. Hughes, Mixed finite element methods—reduced and selective integration techniques: a unification of concepts, Comput. Meths. Appl. Mech. Engrg. 15 (1978) 63–81.
[36] R.D. Mindlin, Influence of rotatory inertia and shear on flexural motions of isotropic, elastic plates, J. Appl. Mech. 18 (1951) 31–38.
[37] P.M. Naghdi, The theory of shells and plates, Mechanics of Solids II, in: C. Truesdell, ed., Vol. VIa/2, pp. 425–640; Encyclopedia of Physics, S. Flügge, ed. (Springer, Berlin/Heidelberg/New York, 1972).
[38] E. Onate, E. Hinton and N. Glover, Techniques for improving the performance of Ahmad shell elements, C/R/313/78, Department of Civil Engineering, University of Wales, Swansea (1978).
[39] B. O'Neill, Elementary differential geometry (Academic Press, New York, 1966).
[40] S.W. Papenfuss, Lateral plate deflection by stiffness matrix methods with application to a marquee, M.S. Thesis, Department of Civil Engineering, University of Washington, Seattle (December 1959).
[41] H. Parisch, Geometrical nonlinear analysis of shells, Comput. Meths. Appl. Mech. Engrg. 14 (1978) 159–178.
[42] H. Parisch, A critical survey of the 9-node degenerated shell element with special emphasis on thin shell application and reduced integration, Comput. Meths. Appl. Mech. Engrg. 20 (1979) 323–350.
[43] L.A. Pars, A treatise on analytical dynamics (Wiley, New York, 1965).
[44] E.D.L. Pugh, E. Hinton and O.C. Zienkiewicz, A study of quadrilateral plate bending elements with 'reduced' integration, Internat. J. Numer. Meths. Engrg. 12(7) (1978) 1059–1079.
[45] E. Ramm, A plate/shell element for large deflection and rotations, in: K.J. Bathe, J.T. Oden and W. Wunderlich, eds., Formulations and computational algorithms in finite element analysis (M.I.T. Press, Cambridge, MA., 1977).

[46] H.L. Schreyer, R.F. Kulak and J.M. Kramer, Accurate numerical solutions for elastic-plastic models, J. Pressure Vessel Technol. 101 (1979) 226–234.
[47] R.L. Taylor, Finite elements for general shell analysis, Preprints of the 5th International Seminar on Computational Aspects of the Finite Element Method, Berlin (West), Germany, August 20–21, 1979.
[48] S. Timoshenko and S. Woinowsky-Krieger, Theory of Plates and Shells (McGraw-Hill, New York, 1959) 2nd ed.
[49] C. Truesdell and W. Noll, The nonlinear field theories of mechanics, Vol. III/3 in: S. Flügge, ed., Encyclopedia of Physics (Springer, Berlin/Heidelberg/New York, 1965).
[50] S. Way, Uniformly loaded, clamped, rectangular plates with large deformation, Proc. 5th International Congress of Applied Mechanics, Cambridge, MA., 1938.
[51] G. Wempner, Finite elements, finite rotations and small strains of flexible shells, Internat. J. Solids and Struct. 5 (1969) 117–153.
[52] R.D. Wood and O.C. Zienkiewicz, Geometrically nonlinear finite element analysis of beams, frames, arches, and axisymmetric shells, Comput. and Struct. 7 (1977) 725–735.
[53] O.C. Zienkiewicz, The finite element method (McGraw-Hill, London, 1977) 3rd ed.
[54] O.C. Zienkiewicz, J. Bauer, K. Morgan and E. Onate, A simple element for axisymmetric shells with shear deformation, Internat. J. Numer. Meths. Engrg. 11 (1977) 1545–1558.
[55] O.C. Zienkiewicz, R.L. Taylor and J.M. Too, Reduced integration technique in general analysis of plates and shells, Internat. J. Numer. Meths. Engrg. 3 (1971) 275–290.